



Mitochondria DNA mutations cause sex-dependent development of hypertension and alterations in cardiovascular function

Mark J. Golob^{a,b}, Lian Tian^a, Zhijie Wang^a, Todd A. Zimmerman^a, Christine A. Caneba^a, Timothy A. Hacker^c, Guoqing Song^c, Naomi C. Chesler^{a,c,*}

^a Department of Biomedical Engineering, UW-Madison College of Engineering, Madison, WI 53706, United States

^b Material Science Program, UW-Madison College of Engineering, Madison, WI 53706, United States

^c Department of Medicine, Medical Science Center, University of Wisconsin-Madison, Madison, WI 53706, United States

ARTICLE INFO

Article history:

Accepted 19 December 2014

Keywords:

Hemodynamics
Elastic modulus
Hypertension
Ventricular function
Mitochondria DNA

ABSTRACT

Aging is associated with conduit artery stiffening that is a risk factor for and can precede hypertension and ventricular dysfunction. Increases in mitochondria DNA (mtDNA) frequency have been correlated with aging. Mice with a mutation in the encoding domain (D257A) of a proof-reading deficient version of mtDNA polymerase- γ (POLG) have musculoskeletal features of premature aging and a shortened lifespan. However, few studies using these mice have investigated the effects of mtDNA mutations on cardiovascular function. We hypothesized that the proof-reading deficient mtDNA POLG leads to arterial stiffening, hypertension, and ventricular hypertrophy. Ten to twelve month-old D257A mice ($n=13$) and age- and sex-matched wild-type controls ($n=13$) were catheterized for hemodynamic and ventricular function measurements. Left common carotid arteries (LCCA) were harvested for mechanical tests followed by histology. Male D257A mice had pulmonary and systemic hypertension, arterial stiffening, larger LCCA diameter (701 ± 45 vs. $597 \pm 60 \mu\text{m}$), shorter LCCA axial length (8.96 ± 0.56 vs. 10.10 ± 0.80 mm), and reduced hematocrit (29.1 ± 6.1 vs. 41.3 ± 8.1 ; all $p < 0.05$). Male and female D257A mice had biventricular hypertrophy ($p < 0.05$). Female D257A mice did not have significant increases in pressure or arterial stiffening, suggesting that the mechanisms of hypertension or arterial stiffening from mtDNA mutations differ based on sex. Our results lend insight into the mechanisms of age-related cardiovascular disease and may point to novel treatment strategies to address cardiovascular mortality in the elderly.

© 2014 Elsevier Ltd. All rights reserved.

1. Introduction

As an increasing portion of US society approaches old age, understanding the mechanisms of age-related cardiovascular disease will be critical. Age-related arterial stiffening is associated with hypertension and ventricular dysfunction and can be an important predictive index for cardiovascular disease (Lee and Oh, 2010). One mechanism for this relationship is mechanical; arterial stiffening can increase systolic blood pressure via an early return of the reflected pressure waves generated from ventricular ejection (Safar et al., 2003). The resulting increased pressures cause endothelial and smooth muscle cell (SMC) dysfunction and arterial collagen accumulation (Eberth et al., 2010; Lee and Oh, 2010) and subsequently increased ventricular afterload (Kelly et al., 1992), which can eventually lead to heart failure.

At the molecular level, aging has been correlated with increased damage and higher mutation frequency of mitochondria DNA (mtDNA) (Dai et al., 2010; Khaidakov et al., 2003; Trifunovic et al., 2004; Wallace, 2010), leading to the hypothesis that mtDNA mutations contribute to mammalian aging (Kujoth et al., 2005) and may play a role in vascular aging. Elevated levels of mtDNA mutations have been documented in transgenic mice that have an alteration in the mitochondria polymerase- γ (POLG) which is responsible for mtDNA replication (Zhang et al., 2000). For example, mice with a homozygous mutation in the encoding domain (D257A) of a proof-reading deficient version of mtDNA POLG have musculoskeletal features of premature aging including kyphosis and sarcopenia as well as a shortened lifespan (~ 13 months) (Kujoth et al., 2005). These transgenic animal studies demonstrated that the accumulation of mtDNA mutations can be pathogenic (Zhang et al., 2000, 2003). However, effects of mtDNA mutations on cardiovascular function in D257A mice have not been fully investigated.

Here, we sought to investigate cardiovascular performance, in particular, hemodynamics, ventricular function, and arterial biomechanics in male and female D257A and wild-type (WT) mice. We

* Corresponding author at: University of Wisconsin at Madison, 2146 Engineering Centers Building, 1550 Engineering Drive, Madison, WI 53706-1609, United States. Tel.: +1 608 265 8920; fax: +1 608 265 9239.

E-mail address: chesler@engr.wisc.edu (N.C. Chesler).

hypothesized that the mitochondrial defect in the mtDNA POLG causes arterial stiffening and adverse hemodynamic effects. To test this, we measured hemodynamics and ventricular function in vivo and measured both structure and function of carotid arteries ex vivo, including frequency-dependent dynamic mechanical properties, which provide a more accurate representation of physiological loading and viscoelastic behavior (Wang et al., 2013b). Our results lend insight into the mechanisms of age-related cardiovascular performance, which may point to novel clinical treatment strategies to address cardiovascular mortality in the elderly.

2. Materials and methods

2.1. Animal handling

Twenty-six mice (male WT $n=7$, male D257A $n=7$, female WT $n=6$, female D257A $n=6$), 10–12 months old, were obtained from an established colony (Kujoth et al., 2005). All procedures were approved by the University of Wisconsin-Madison Institutional Animal Care and Use Committee.

2.2. Echocardiography

Body weight (BW) was measured, and then mice were anesthetized with isoflurane (1%) and maintained at 37 °C via a heated platform. Transthoracic echocardiography was performed with a 30-MHz transducer (RMV 707B, Visual Sonics, Toronto) (Brody et al., 2012; Harris et al., 2002). Two-dimensionally guided M-mode and Doppler images were acquired at the tip of the papillary muscles in the left ventricle (LV) to assess ventricular function. From these images, LV and septum (S) mass were estimated ($LV_{iv}+S$, in vivo) and the common carotid artery blood flow velocity and length were measured. Diastolic function was assessed by isovolumic relaxation time (IVRT). Systolic function was evaluated by endocardial fractional shortening (%FS). All parameters were obtained over at least three consecutive heartbeats.

2.3. Hemodynamic measurements

Mice were anesthetized via urethane (1.6 mg/g body weight, i.p.), and the chest was opened for pressure–volume (PV) measurements using a 1.2 F admittance catheter (Schreier et al., 2013; Tabima et al., 2010). LV function was measured at baseline, and then the PV catheter was placed into the right ventricle (RV) to assess RV function at baseline. For LV and RV measurements, the inferior vena cava was occluded at least three times to alter preload. Synchronized pressure and volume waveforms were recorded by commercial software (Notocord, Croissy Sur Seine, France). Analysis included at least 10 consecutive cardiac cycles.

Cardiac output (CO), stroke volume (SV), heart rate (HR), and RV, LV, and aortic pressures were quantified. Systolic function was assessed via the ejection fraction (EF) and the maximum derivative of pressure (dP/dt_{max}) (Joho et al., 2007); diastolic function by the minimum derivative of pressure (dP/dt_{min}) and relaxation factor τ (Tabima et al., 2010); vascular function by effective arterial elastance (E_a) (Kelly et al., 1992); and ventricular contractile function by load-independent indices including end-systolic elastance (E_{es}), preload recruitable stroke work (PRSW), and $dP/dt_{max} - V_{ed}$ (Pacher et al., 2008).

2.4. Tissue harvest

After in vivo measurements, animals were euthanized, and a blood sample was drawn to measure hematocrit (Hct). The left common carotid arteries (LCCA) were excised, submerged in saline, and placed on ice. The RV free wall, LV free wall and septum were weighed to calculate the Fulton index ($FI=RV/(LV+S)$), an index of RV hypertrophy (Ciuculan et al., 2011; Wang et al., 2013b). The LV mass-to-BW ratio ($(LV+S)/BW$) was calculated as an index of LV hypertrophy (Ding et al., 2000; Mazzolai et al., 2000).

2.5. Isolated vessel mechanical test

The LCCA was mounted in a vessel chamber in pH-adjusted physiological saline solution (PSS) as previously described (Wang and Chesler, 2012; Wang et al., 2013b). The LCCA was stretched 150% axially to mimic in vivo length (Tian et al., 2013; Wang et al., 2013a), pressurized to 90 mmHg, and allowed to equilibrate at 37 °C for 30 min. Sinusoidal pressure cycles of 90–120 mmHg at 1 Hz were applied for pre-conditioning to achieve a consistent mechanical response (Fung et al., 1979).

2.6. Active state

U46619 (Cayman Chemical, Ann Arbor, MI), a thromboxane analog, was added to the superfusate to induce vasoconstriction (concentration of 1.5×10^{-7} M). The outer diameter (OD) at 90 mmHg was recorded at several time points between 0 and 30 min after drug infusion. Then, vasoactivity was calculated as the percent change in diameter as done previously (Ooi et al., 2010):

$$\% \Delta OD = \left(\frac{OD_t - OD_i}{OD_i} \right) \times 100 \quad (1)$$

where OD_t is the OD at time t and OD_i is the initial OD before U46619 addition

2.7. Passive state

After active-state testing, the superfusate was replaced with Ca^{2+} - and Mg^{2+} -free physiological buffer solution (PBS), and the vessel was equilibrated and preconditioned using the same conditions. Wall thickness (h) and OD were measured optically at 120 mmHg and 5 mmHg with the latter taken as the no-load state (Ooi et al., 2010). For static mechanical testing, the vessel was initially pressurized to 90 mmHg. Then, the pressure was increased in 5 mmHg increments and held for a minimum of 30 s up to 120 mmHg with OD recorded at each pressure. Dynamic testing was performed at 90–120 mmHg at 0.01, 0.1, 1, 3, 5, 8, and 10 Hz.

2.8. Mechanical property analysis

The arteries were assumed to be incompressible, and results are reported using measurements with PBS perfusion. Wall thickness as a function of pressure was calculated assuming conservation of mass and no axial extension (Faury et al., 1999; Ooi et al., 2010):

$$h = \frac{1}{2} \left[OD - \sqrt{OD^2 - OD_{120}^2 + (OD_{120} - 2h_{120})^2} \right] \quad (2)$$

where OD_{120} and h_{120} are the OD and h measured at 120 mmHg, respectively.

The stretch ratio (Ooi et al., 2010) was calculated as follows:

$$\lambda = \frac{OD_p}{OD_5} \quad (3)$$

where OD_p is the OD measurement at each pressure step, and OD_5 is the OD measurement at 5 mmHg under PBS. Circumferential stress (σ) was calculated using the thin-walled assumption as done previously for carotid arteries (Dye et al., 2007; Tian et al., 2013):

$$\sigma = \frac{Pr}{h} \quad (4)$$

where P is the transmural pressure and h and r are respectively the arterial wall thickness and the inner radius. 2nd Piola–Kirchhoff stress (S) and Green strain (ϵ) were calculated as follows:

$$S = \frac{\sigma}{\lambda^2} \quad (5)$$

$$\epsilon = \frac{1}{2} (\lambda^2 - 1) \quad (6)$$

where λ is the stretch ratio. From the stress–strain data, elastic modulus was calculated by the slope of the line best-fit to the Kirchhoff stress–Green strain hysteresis generated by loading and unloading cycles. Damping was quantified by the ratio of dissipated to stored energy using the hysteresis area as done previously (Wang and Chesler, 2012; Wang et al., 2013b).

2.9. Histology and immunohistochemistry

After mechanical testing, the LCCA was stored in 10% formalin. The vessels were embedded in paraffin, sectioned, and stained with picrosirius red (SR). Images were captured using an inverted microscope (TE-2000-5, Nikon, Melville, NY) and analyzed using MetaVue (Optical Analysis Systems, Nashua, NH). For the SR stains, the area containing collagen was identified by color thresholding in a representative field of view (containing the entire vessel) by an observer blinded to the experimental condition. The collagen area was then divided by the total tissue area to calculate collagen percent in the arterial wall.

To measure eNOS expression in LCCAs, immunohistochemistry was performed following standard protocols using primary antibodies for eNOS (Thermo Scientific, PA1-037) at a dilution of 1:100. The secondary antibody used was a goat anti-rabbit IgG (Life Technologies, A-21244). Staining was imaged and then quantified with a Nikon Eclipse Ti inverted microscope. For quantification, the eNOS expression level was represented by the relative area positive for eNOS normalized by the area positive for DAPI using NIH software (ImageJ 1.48).

2.10. Western blot

Quantification of angiotensin-II type 1 receptor was performed via western blotting. Ventricular tissue specimens were homogenized using Abcam western blot tissue homogenization protocols. Tissue was weighed and added to RIPA buffer with inhibitors and homogenized using a handheld tissue homogenizer (Fisher Scientific). The tissue was then kept in 4 °C with constant agitation for 2 h, centrifuged, and stored in –20 °C. Gel electrophoresis and blotting were performed as described previously (Rodriguez et al., 2014). Briefly, 20 µg of each sample was loaded onto a gel (NuPAGE, Life Technologies) and run at 220 V for 50 min. After transferring the proteins, membranes were incubated with primary antibodies (Anti-angiotensin-II type 1 receptor, AbCam, 18801), an antibody against GAPDH (Cell Signaling, 2118L), and a secondary antibody goat anti-rabbit (Li-Cor, IRDye 800CW). The blot was imaged using Li-Cor technology, and band intensity was determined using NIH software (ImageJ 1.48).

2.11. Statistics

Results are reported as mean \pm SD. Statistical significance was assessed using a two-way ANOVA for sex and strain (R, Foundation for Statistical Computing, USA, version 3.0.1), and significance was taken at a two-sided *p*-Value less than 0.05. Tukey multiple comparisons were used for post-hoc analysis (R).

3. Results

3.1. Tissue weights, arterial dimensions, and hematocrit

We evaluated differences in tissue weights, hematocrit, and arterial geometry caused by mtDNA mutations and sex. All D257A mice had lower body weight (Fig. 1A) and higher FI and LV+S to BW ratios, demonstrating biventricular hypertrophy (Fig. 1B–D). The larger diameter and lower axial lengths indicate carotid artery geometric changes (Fig. 1E–H). However, wall thickness was not different between any of the groups (data not shown). Finally, we observed a lower hematocrit in D257A mice (Fig. 1I).

3.2. Vasoactivity, morphology, and protein expression

Ex vivo, LCCAs exhibited significant constriction in response to U46619 (male WT $-25 \pm 9\%$; male D257A $-31 \pm 12\%$; female WT $-33 \pm 13\%$; female D257A $-35 \pm 13\%$; $p < 0.05$ vs. normal SMC tone). Vasoactivity was not different between male WT and male D257A nor between female WT and female D257A mice. Representative Sirius red-stained images of arteries of male mice are illustrated in Fig. 2A (left, WT; right, D257A). Quantitative analysis of collagen staining indicated that only male D257A carotid arteries had higher collagen content compared to WT mice (Fig. 2B). H&E staining demonstrated intact endothelial and smooth muscle cells as well as defined elastic layers in the media for all mice (data not shown). Expressions of eNOS in the carotids and angiotensin-II type 1 receptor in the ventricles were not different between WT and D257A mice (data not shown).

3.3. Hemodynamics and ventricular function

Hemodynamics and ventricular function were measured to determine the global cardiovascular consequences of the mtDNA mutation in mice. Aortic pressures, end-systolic pressures, and LCCA blood flow velocity were only significantly higher in male D257A mice (Fig. 3). Table 1 shows that mitral valve velocity and load-independent and load-dependent indices were only higher for male D257A mice. These results indicate that the mtDNA mutation had a sex-dependent effect since the differences were not significant in female mice.

3.4. Arterial mechanics

Since arteries are viscoelastic, we measured mechanical properties in static and dynamic conditions. In static tests, we observed a larger elastic modulus in male D257A mice (Fig. 4A). In dynamic tests, all stress–strain curves exhibited a hysteresis, indicating energy dissipation. Modulus and damping exhibited little frequency dependence, and, while D257A mice modulus tended to be higher than WT at all frequencies for both sexes, no significant differences in modulus were observed between strains or sexes at any frequency (Fig. 4B).

4. Discussion

This study presents the first in-depth measurements of hemodynamics, ventricular function, and arterial stiffness in the POLG mouse model generated with mtDNA mutations. Our main finding is that mtDNA mutations led to sex differences in blood pressure, ventricular function, and carotid artery stiffness, which indicates a possible role of female hormones in mtDNA-mediated cardiovascular performance changes. D257A mice also had changes in carotid artery diameter, length, and collagen content. These results suggest that mtDNA mutations are involved in cardiovascular diseases such as hypertrophy and hypertension, and therapies may be tailored to target pathways related with mtDNA mutations.

Systemic and pulmonary hypertension were observed in this study, and this is consistent with biventricular hypertrophy and heart enlargement (Zhang et al., 2000, 2003) previously reported in mice with mtDNA mutations, but the prior studies did not examine changes in ventricular function or arterial pressure. Left and right ventricular hypertrophy (Fig. 1B–D) was coincident with and likely caused by systemic (Fig. 3A–D) and pulmonary (Fig. 3E) hypertension, respectively in D257A mice.

Our results also show that hematocrit was lower in D257A mice (Fig. 1I). Although others have shown a decrease in hematocrit in D257A mice at 6 (Trifunovic et al., 2004), 9 (Kujoth et al., 2005), and 10 (Dillon et al., 2012) months, we provide the first indication that this may have implications for hemodynamics. In particular, decreased hematocrit results in a lower blood viscosity at a given shear rate (Simmonds et al., 2013), which lowers wall shear stress. To maintain homeostasis, arteries likely underwent constriction and narrowing. Thus, the increased vascular resistance that likely increased blood pressure may have been stimulated by decreased hematocrit. This finding is also important considering altered blood rheology parameters are independent predictors of cardiovascular health (Feher et al., 2006). Future studies may help elucidate the pathogenic effect of mtDNA mutations on blood rheology.

The metrics of ventricular function derived from PV loops show that cardiac function was comparable between wild-type and D257A mice (Table 1). It is well known that the heart remodels to adapt to changes in loading conditions such as elevated pressure from exercise or hypertension (Borgdorff et al., 2013). In this case, ventricular hypertrophy likely occurred as a response to increased afterload as evidenced by a larger E_a . We speculate that the observed hypertrophy in female mice was adaptive and successfully compensated for the increased load quantified by the load-dependent metrics of ventricular function (Table 1). In an experimental model of pulmonary hypertension, both placebo and estrogen-treated ovariectomized female mice had ventricular hypertrophy, but estrogen improved right ventricular contractility while limiting afterload and pulmonary vascular stiffening (Liu et al., 2014).

The absence of ventricular dysfunction in the D257A mice may be attributed to several factors. First, whereas there is evidence of significant musculoskeletal defects in D257A mice at 9 months of age (Kujoth et al., 2005), the rate of accumulation of mtDNA

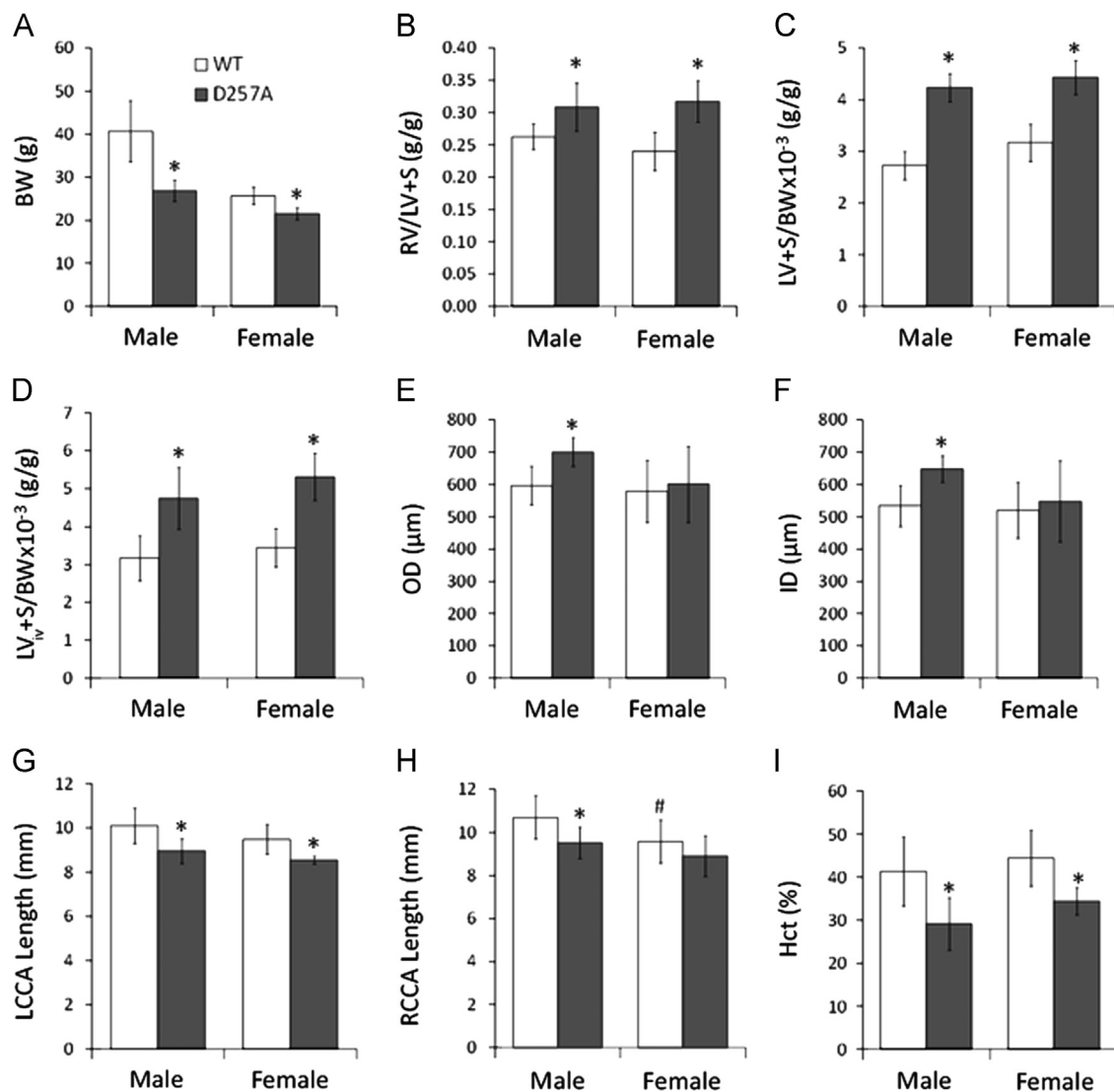


Fig. 1. Body weight, ventricular hypertrophy indices, arterial diameters, and hematocrit for WT and D257A male and female mice. A: Body weight. B: RV/LV+S; Fulton index. C: LV+S to BW ratio (ex vivo tissue harvest). D: LV+S to BW ratio (in vivo). E: LCCA outer diameter at 120 mmHg under PBS. F: LCCA inner diameter at 120 mmHg under PBS. G: Left common carotid artery length. H: Right common carotid artery (RCCA) length. I: Hematocrit. * $p < 0.05$ vs. WT of the same sex, # $p < 0.05$ vs. male of the same genotype.

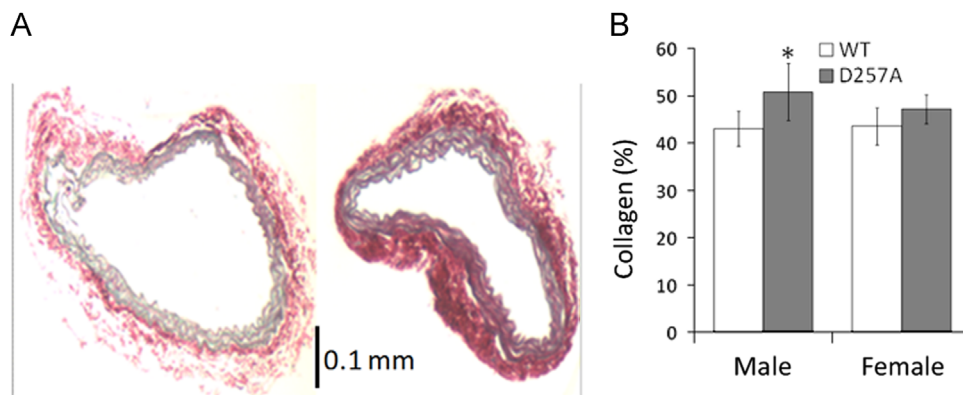


Fig. 2. Histological staining of WT and D257A mice. A: Representative cross sections of male WT (left) and male D257A (right) LCCA stained with SR. B: Collagen content by quantitative analysis of SR staining. * $p < 0.05$ vs. WT of the same sex.

mutations may be lower in the heart compared to musculoskeletal and other tissues (Vermulst et al., 2008). For example, Edgar et al. found that the magnitude of the reduction in the mitochondria electron transport complex activity was smaller in the heart

compared to liver tissue in these mice (Edgar et al., 2009). Vermulst et al. found a higher mtDNA mutation frequency in the brain compared to that observed in the heart (Vermulst et al., 2007). Another explanation may be based on the concept of a mtDNA

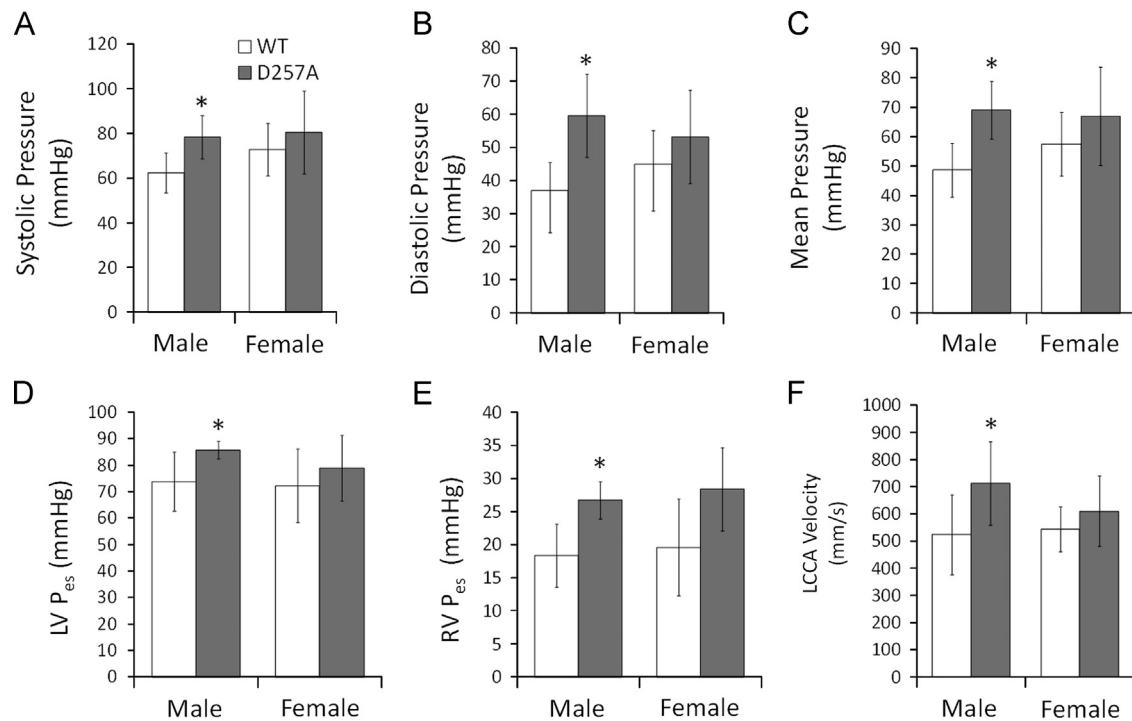


Fig. 3. Hemodynamics and ventricular function for WT and D257A male and female mice. A: Aortic systolic pressure. B: Aortic diastolic pressure. C: Mean aortic pressure. D: LV end-systolic pressure. E: RV end-systolic pressure. F: Left common carotid artery velocity. * $p < 0.05$ vs. WT of the same sex.

mutation threshold. The threshold effect theory holds that a minimum number of mtDNA mutations must be present before mitochondria dysfunction occurs and aging phenotypes become apparent (DiMauro and Schon, 2003). Our results suggest that cardiovascular tissue may have a higher threshold compared to musculoskeletal tissue. Therefore, the mild phenotypes we observed in the cardiovascular system may be a result of a lower rate of mtDNA accumulation and higher threshold for mtDNA mutations.

D257A mice exhibited several alterations in morphometric parameters in the systemic vasculature. We found that the in vivo axial carotid artery length was smaller in D257A mice (Fig. 1G and H). Axial remodeling has been observed in mice with elevated pressures from an aortic banding procedure (Eberth et al., 2010). This length reduction may be a mechanism to compensate for the circumferential remodeling (Humphrey et al., 2009) or simply a result of the higher pressures that cause more circumferential than axial stretch due to known differences in circumferential and axial elastic moduli (Dobrin and Doyle, 1970; Guo and Kassab, 2003; Tanaka and Fung, 1974). Ex vivo, at the same transmural pressure, carotid artery diameter was higher in D257A mice (Fig. 1E and F), and increased diameter has previously been observed to be an age-related phenotype (Hausman et al., 2012). The larger diameter in D257A mice may be a result of chronically increased pressure (Fig. 3A–C), increased blood flow velocity (Fig. 3F), which could cause flow-induced vasodilation and enlargement, or both. While these changes, like those in pressure and ventricular function, are mild, our data for the first time indicate that the accumulation of mtDNA mutations in the systemic vasculature results in carotid artery morphometric changes, which are implicated in remodeling from hypertension.

Arterial stiffening has long been associated with hypertension, either as a consequence of elevated pressures (Ooi et al., 2010) or a cause (Weisbrod et al., 2013), so we expected to see stiffer arteries in D257A mice. From static mechanical tests, we observed a significantly larger elastic modulus in male D257A compared to male WT mice (Fig. 4A), which may be attributed to the higher collagen content in the LCCA (Fig. 2B). Interestingly, the increase in

static elastic modulus was not significant in female D257A mice. A trend of LCCA stiffening was observed in male and female D257A mice from the dynamic mechanical tests (Fig. 4B), although the changes did not reach statistical significance. Elastic modulus values were slightly higher in static compared to dynamic conditions, which is consistent with a previous investigation on rat carotid arteries where the slope of the static pressure–diameter curve was steeper than that in the dynamic condition (Glaser et al., 1995). The development of systemic hypertension with the stiffening observed here suggests that, at least in this mouse model, arterial stiffening may be a factor underlying the pathogenesis of hypertension. Given the hemodynamic, mechanical, and structural changes, this mouse model may be a useful addition into a meta-analysis of other murine models to further understand the effects of genetic mutations on the hemodynamics, structure, and biomechanics of blood vessels (Bersi et al., 2014).

Our findings indicate that the mtDNA mutation had a greater impact on males. Although the trends were the same in females, body weight and hematocrit were only significantly lower and arterial diameter was only significantly higher in male D257A mice (Fig. 1). Similarly, aortic pressures, ventricular pressures, LCCA velocity, and E_a were only significantly higher in male D257A mice (Fig. 3, Table 1), suggesting that female mice with this mutation were protected against premature aging phenotypes and hypertension resulting from mtDNA mutations. The development of hypertension in rodents induced via angiotensin-II (Xue et al., 2005), hypobaric hypoxia (Rabinovitch et al., 1981), a kidney wrap (Haywood and Hinojosa-Laborde, 1997), and a renal artery clip (Wolinsky, 1971) was less in females compared to males. Similarly, recovery in female rats was more pronounced than in male rats (Wolinsky, 1971). Moreover, as noted above, estrogen limited pulmonary arterial stiffening and improved ventricular contractility in a rodent model of pulmonary hypertension (Liu et al., 2014). These results indicate that hormonal factors may mediate the mechanisms causing hypertension.

To identify potential sex-dependent mechanisms of mtDNA mutation-induced systemic and pulmonary hypertension,

Table 1

Ventricular function metrics for WT male (M) and female (F) and D257A male and female mice.

Strain Sex	WT M	D257A M	WT F	D257A F
<i>Left ventricle</i>				
<i>Ventricular function</i>				
HR [beats/min]	507 ± 49	479 ± 93	505 ± 63	521 ± 47
SV [μL]	16 ± 2	14 ± 2	16 ± 5	17 ± 4
CO [μL/min]	9010 ± 2413	6926 ± 1573	8277 ± 2644	8962 ± 2319
<i>Diastolic function</i>				
dP/dt _{min} [mmHg/s]	−4468 ± 1082	−6415 ± 813*	−5100 ± 1177	−6631 ± 1032
τ [ms]	7.8 ± 1.3	6.8 ± 0.8	8.5 ± 3.1	5.8 ± 1.8
MVE [mm/s]	733 ± 80	949 ± 91*	674 ± 95	866 ± 84*
MVA [mm/s]	518 ± 41	624 ± 10*	509 ± 136	516 ± 29*
IVRT [ms]	19 ± 1	18 ± 3	19 ± 2	19 ± 2
MV E/A	1.42 ± 0.22	1.49 ± 0.23	1.49 ± 0.33	1.57 ± 0.03
<i>Systolic function</i>				
EF [%]	61 ± 11	74 ± 7	66 ± 16	54 ± 7 [#]
dP/dt _{max} [mmHg/s]	7298 ± 2042	9020 ± 984	7455 ± 1897	9166 ± 196
dP/dt _{max} − V _{ed} [mmHg/μLs]	259 ± 90	474 ± 71*	211 ± 27	324 ± 101
FS [%]	33 ± 2	38 ± 10	32 ± 5	36 ± 4
<i>Vascular indices</i>				
E _a	4.34 ± 0.77	6.23 ± 0.87*	4.02 ± 1.08	4.45 ± 0.86
<i>Contractility</i>				
E _{es} [mmHg/μL]	5.5 ± 1.6	7.1 ± 3.7	7.2 ± 1.2	8.4 ± 2.2
PRSW [mmHg]	93 ± 26	108 ± 36	104 ± 59	105 ± 40
<i>Right ventricle</i>				
<i>Ventricular function</i>				
HR [beats/min]	493 ± 32	438 ± 71	522 ± 51	512 ± 63
SV [μL]	14 ± 2	13 ± 2	8 ± 6	11 ± 4
CO [μL/min]	6900 ± 1022	5442 ± 1285	4352 ± 2897	5574 ± 2063
<i>Diastolic function</i>				
dP/dt _{min} [mmHg/s]	−1540 ± 134	−1755 ± 325	−1429 ± 388	−2208 ± 119*
τ [ms]	5.3 ± 1.5	7.3 ± 2.1	4.0 ± 1.6	5.0 ± 2.8
<i>Systolic function</i>				
EF [%]	39 ± 5	37 ± 9	42 ± 20	36 ± 6
dP/dt _{max} [mmHg/s]	1885 ± 204	2108 ± 683	2055 ± 932	2662 ± 296
dP/dt _{max} − V _{ed} [mmHg/μLs]	53 ± 7	42 ± 18	77 ± 32	72 ± 10
<i>Vascular indices</i>				
E _a	1.44 ± 0.50	1.99 ± 0.85	2.82 ± 1.30	2.98 ± 0.85
<i>Contractility</i>				
E _{es} [mmHg/μL]	0.9 ± 0.3	1.0 ± 0.3	1.5 ± 0.5	1.8 ± 0.5
PRSW [mmHg]	14 ± 7	17 ± 12	24 ± 16	18 ± 5

MVE=mitral valve velocity in early diastole; MVA=mitral valve velocity in late diastole; IVRT=isovolumic relaxation time; MV E/A=ratio of early to late diastolic filling velocities; E_a=effective arterial elastance; HR=heart rate; SV=stroke volume; EF=ejection fraction; CO=cardiac output; SW=stroke work; E_{es}=end-systolic elastance; PRSW=preload recruitable stroke work; FS=fractional shortening.

* $p < 0.05$ vs. WT of the same gender,

[#] $p < 0.05$ vs. male of the same genotype.

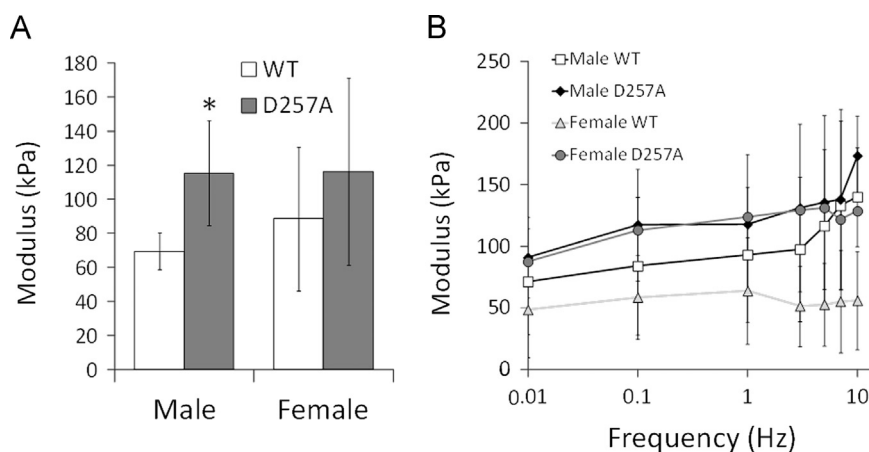


Fig. 4. Mechanical properties of LCCA for WT and D257A male and female mice. A: Static elastic modulus. B: Dynamic elastic modulus as a function of frequency obtained in SMC passive state. * $p < 0.05$ vs. WT of the same sex.

we examined the expression of eNOS and angiotensin-II type 1 receptor. Both the nitric oxide and angiotensin-II pathways are well known to be modulated by estrogen (Kim and Levin, 2006; Sudar et al., 2008). We found that expression levels of neither eNOS in the carotids nor angiotensin-II type 1 receptor in the ventricles were different between WT and D257A mice. We were not able to examine the circulating angiotensin expressions in the present study but it may be increased in the D257A mice despite equivalent levels of angiotensin-II receptors. Discovering the sex-dependent pathways by which mtDNA mutations contribute to hypertension will be the focus of future work.

4.1. Limitations

Distal systemic and pulmonary arteries were not examined in this study as the carotid arteries were the main focus, and distal artery mechanics in mice are difficult to study *ex vivo* due to their small size. Distal artery narrowing may be responsible for the systemic and pulmonary artery pressure increases found here and warrant future study. In addition, mitochondria are different in pulmonary vs. systemic arteries (Dromparis et al., 2010), so the effects of mtDNA mutations may differ in the two circulations. Further research is necessary to quantify the heterogeneity of the effects and rates of mtDNA mutations in cardiovascular tissues.

4.2. Conclusion

Mitochondrial defects are implicated in cardiovascular disease and our results show that mtDNA mutations cause systemic and pulmonary hypertension and bi-ventricular hypertrophy. We observed sex differences, which suggest that sex hormones may affect the mechanisms that cause hypertension from mtDNA mutations. The relatively mild cardiovascular effects of these mutations, in contrast to previously reported dramatic musculoskeletal changes, suggest significant heterogeneity in the impact of mtDNA mutations and possibly in mitochondria function in different tissues with aging. The molecular mechanisms of difference in rates of cardiovascular aging and musculoskeletal aging are an important direction for future research.

Conflict of interest

No conflicts of interest are declared by the authors.

Acknowledgments

This work was supported by NIH Grant 1R01HL086939 (NCC) and T32 HL-07936-13 (CAC). We gratefully acknowledge Professor Tomas A. Prolla for providing the WT and D257A mice used in this study. We would also like to thank Dr. Stephanie Morgan for help with immunohistochemistry imaging and Chloe Kim for help with Western blot techniques.

References

- Bersi, M.R., Ferruzzi, J., Eberth, J.F., Gleason Jr., R.L., Humphrey, J.D., 2014. Consistent biomechanical phenotyping of common carotid arteries from seven genetic, pharmacological, and surgical mouse models. *Ann. Biomed. Eng.* 42, 1207–1223.
- Borgdorff, M.A., Bartelds, B., Dickinson, M.G., Steendijk, P., de Vroomen, M., Berger, R.M., 2013. Distinct loading conditions reveal various patterns of right ventricular adaptation. *Am. J. Physiol.: Heart Circ. Physiol.* 305, H354–H364.
- Brody, M.J., Hacker, T.A., Patel, J.R., Feng, L., Sadoshima, J., Tevosian, S.G., Balijepalli, R.C., Moss, R.L., Lee, Y., 2012. Ablation of the cardiac-specific gene leucine-rich repeat containing 10 (Lrrc10) results in dilated cardiomyopathy. *PLoS One* 7, e51621.
- Ciucian, L., Bonneau, O., Hussey, M., Duggan, N., Holmes, A.M., Good, R., Stringer, R., Jones, P., Morrell, N.W., Jarai, G., Walker, C., Westwick, J., Thomas, M., 2011. A novel murine model of severe pulmonary arterial hypertension. *Am. J. Respir. Crit. Care Med.* 184, 1171–1182.
- Dai, D.F., Chen, T., Wanagat, J., Laflamme, M., Marcinek, D.J., Emond, M.J., Ngo, C.P., Prolla, T.A., Rabinovitch, P.S., 2010. Age-dependent cardiomyopathy in mitochondrial mutator mice is attenuated by overexpression of catalase targeted to mitochondria. *Aging Cell* 9, 536–544.
- Dillon, L.M., Williams, S.L., Hida, A., Peacock, J.D., Prolla, T.A., Lincoln, J., Moraes, C.T., 2012. Increased mitochondrial biogenesis in muscle improves aging phenotypes in the mtDNA mutator mouse. *Hum. Mol. Genet.* 21, 2288–2297.
- DiMauro, S., Schon, E.A., 2003. Mitochondrial respiratory-chain diseases. *N. Engl. J. Med.* 348, 2656–2668.
- Ding, B., Price, R.L., Goldsmith, E.C., Borg, T.K., Yan, X., Douglas, P.S., Weinberg, E.O., Bartunek, J., Thielens, T., Didenko, V.V., Lorell, B.H., 2000. Left ventricular hypertrophy in ascending aortic stenosis mice: anoxia and the progression to early failure. *Circulation* 101, 2854–2862.
- Dobrin, P.B., Doyle, J.M., 1970. Vascular smooth muscle and the anisotropy of dog carotid artery. *Circ. Res.* 27, 105–119.
- Dromparis, P., Sutendra, G., Michelakis, E.D., 2010. The role of mitochondria in pulmonary vascular remodeling. *J. Mol. Med.* 88, 1003–1010.
- Dye, W.W., Gleason, R.L., Wilson, E., Humphrey, J.D., 2007. Altered biomechanical properties of carotid arteries in two mouse models of muscular dystrophy. *J. Appl. Physiol.* 103, 664–672.
- Eberth, J.F., Popovic, N., Gresham, V.C., Wilson, E., Humphrey, J.D., 2010. Time course of carotid artery growth and remodeling in response to altered pulsatility. *Am. J. Physiol.: Heart Circ. Physiol.* 299, H1875–H1883.
- Edgar, D., Shabalina, I., Camara, Y., Wredenberg, A., Calvaruso, M.A., Nijtmans, L., Nedergaard, J., Cannon, B., Larsson, N.G., Trifunovic, A., 2009. Random point mutations with major effects on protein-coding genes are the driving force behind premature aging in mtDNA mutator mice. *Cell Metab.* 10, 131–138.
- Faury, G., Maher, G.M., Li, D.Y., Keating, M.T., Mecham, R.P., Boyle, W.A., 1999. Relation between outer and luminal diameter in cannulated arteries. *Am. J. Physiol.* 277, H1745–H1753.
- Feher, G., Koltai, K., Kesmarky, G., Szapary, L., Juricskay, I., Toth, K., 2006. Hemorheological parameters and aging. *Clin. Hemorheol. Microcirc.* 35, 89–98.
- Fung, Y.C., Fronek, K., Patitucci, P., 1979. Pseudoelasticity of arteries and the choice of its mathematical expression. *Am. J. Physiol.* 237, H620–H631.
- Glaser, E., Lacolley, P., Boutouyrie, P., Sacunha, R., Lucet, B., Safar, M.E., Laurent, S., 1995. Dynamic versus static compliance of the carotid artery in living wistar-kyoto rats. *J. Vasc. Res.* 32, 254–265.
- Guo, X., Kassab, G.S., 2003. Variation of mechanical properties along the length of the aorta in c57bl/6 mice. *Am. J. Physiol.: Heart Circ. Physiol.* 285, H2614–H2622.
- Harris, S.P., Bartley, C.R., Hacker, T.A., McDonald, K.S., Douglas, P.S., Greaser, M.L., Powers, P.A., Moss, R.L., 2002. Hypertrophic cardiomyopathy in cardiac myosin binding protein-c knockout mice. *Circ. Res.* 90, 594–601.
- Hausman, N., Martin, J., Taggart, M.J., Austin, C., 2012. Age-related changes in the contractile and passive arterial properties of murine mesenteric small arteries are altered by caveolin-1 knockout. *J. Cell. Mol. Med.* 16, 1720–1730.
- Haywood, J.R., Hinojosa-Laborde, C., 1997. Sexual dimorphism of sodium-sensitive renal-wrap hypertension. *Hypertension* 30, 667–671.
- Humphrey, J.D., Eberth, J.F., Dye, W.W., Gleason, R.L., 2009. Fundamental role of axial stress in compensatory adaptations by arteries. *J. Biomech.* 42, 1–8.
- Joho, S., Ishizaka, S., Sievers, R., Foster, E., Simpson, P.C., Grossman, W., 2007. Left ventricular pressure–volume relationship in conscious mice. *Am. J. Physiol.: Heart Circ. Physiol.* 292, H369–H377.
- Kelly, R.P., Ting, C.T., Yang, T.M., Liu, C.P., Maughan, W.L., Chang, M.S., Kass, D.A., 1992. Effective arterial elastance as index of arterial vascular load in humans. *Circulation* 86, 513–521.
- Khaidakov, M., Heflich, R.H., Manjanatha, M.G., Myers, M.B., Aidoo, A., 2003. Accumulation of point mutations in mitochondrial DNA of aging mice. *Mutat. Res.* 526, 1–7.
- Kujoth, G.C., Hiona, A., Pugh, T.D., Someya, S., Panzer, K., Wohlgemuth, S.E., Hofer, T., Seo, A.Y., Sullivan, R., Jobling, W.A., Morrow, J.D., Van Remmen, H., Sedivy, J.M., Yamasoba, T., Tanokura, M., Weindrich, R., Leeuwenburgh, C., Prolla, T.A., 2005. Mitochondrial DNA mutations, oxidative stress, and apoptosis in mammalian aging. *Science* 309, 481–484.
- Kim, J.K., Levin, E.R., 2006. Estrogen signaling in the cardiovascular system. *Nucl. Recept. Signal.* 4, e013.
- Lee, H.Y., Oh, B.H., 2010. Aging and arterial stiffness. *Circ. J.* 74, 2257–2262.
- Liu, A., Schreier, D., Tian, L., Eickhoff, J.C., Wang, Z., Hacker, T.A., Chesler, N.C., 2014. Direct and indirect protection of right ventricular function by estrogen in an experimental model of pulmonary arterial hypertension. *Am. J. Physiol.: Heart Circ. Physiol.* 307, H273–H283.
- Mazzolai, L., Pedrazzini, T., Nicoud, F., Gabbiani, G., Brunner, H.R., Nussberger, J., 2000. Increased cardiac angiotensin II levels induce right and left ventricular hypertrophy in normotensive mice. *Hypertension* 35, 985–991.
- Ooi, C.Y., Wang, Z., Tabima, D.M., Eickhoff, J.C., Chesler, N.C., 2010. The role of collagen in extralobar pulmonary artery stiffening in response to hypoxia-induced pulmonary hypertension. *Am. J. Physiol.: Heart Circ. Physiol.* 299, H1823–H1831.
- Pacher, P., Nagayama, T., Mukhopadhyay, P., Batkai, S., Kass, D.A., 2008. Measurement of cardiac function using pressure–volume conductance catheter technique in mice and rats. *Nat. Protoc.* 3, 1422–1434.
- Rabinovitch, M., Gamble, W.J., Miettinen, O.S., Reid, L., 1981. Age and sex influence on pulmonary hypertension of chronic hypoxia and on recovery. *Am. J. Physiol.* 240, H62–H72.

- Rodriguez, K.J., Piechura, L.M., Porras, A.M., Masters, K.S., 2014. Manipulation of valve composition to elucidate the role of collagen in aortic valve calcification. *BMC Cardiovasc. Disord.* 14, 29.
- Safar, M.E., Levy, B.I., Struijker-Boudier, H., 2003. Current perspectives on arterial stiffness and pulse pressure in hypertension and cardiovascular diseases. *Circulation* 107, 2864–2869.
- Schreier, D., Hacker, T., Song, G., Chesler, N., 2013. The role of collagen synthesis in ventricular and vascular adaptation to hypoxic pulmonary hypertension. *J. Biomech. Eng.* 135, 021018 (–021018).
- Simmonds, M.J., Meiselman, H.J., Baskurt, O.K., 2013. Blood rheology and aging. *J. Geriatr. Cardiol.* 10, 291–301.
- Sudar, E., Velebit, J., Gluvic, Z., Zakula, Z., Lazic, E., Vuksanovic-Topic, L., Putnikovic, B., Neskovic, A., Isenovic, E.R., 2008. Hypothetical mechanism of sodium pump regulation by estradiol under primary hypertension. *J. Theor. Biol.* 251, 584–592.
- Tabima, D.M., Hacker, T.A., Chesler, N.C., 2010. Measuring right ventricular function in the normal and hypertensive mouse hearts using admittance-derived pressure–volume loops. *Am. J. Physiol.: Heart Circ. Physiol.* 299, H2069–H2075.
- Tanaka, T.T., Fung, Y.C., 1974. Elastic and inelastic properties of the canine aorta and their variation along the aortic tree. *J. Biomech.* 7, 357–370.
- Tian, L., Wang, Z., Lakes, R.S., Chesler, N.C., 2013. Comparison of approaches to quantify arterial damping capacity from pressurization tests on mouse conduit arteries. *J. Biomech. Eng.* 135, 54504.
- Trifunovic, A., Wredenberg, A., Falkenberg, M., Spelbrink, J.N., Rovio, A.T., Bruder, C.E., Bohlooly, Y.M., Gidlof, S., Oldfors, A., Wibom, R., Tornell, J., Jacobs, H.T., Larsson, N.G., 2004. Premature ageing in mice expressing defective mitochondrial DNA polymerase. *Nature* 429, 417–423.
- Vermulst, M., Bielas, J.H., Kujoth, G.C., Ladiges, W.C., Rabinovitch, P.S., Prolla, T.A., Loeb, L.A., 2007. Mitochondrial point mutations do not limit the natural lifespan of mice. *Nat. Genet.* 39, 540–543.
- Vermulst, M., Wanagat, J., Kujoth, G.C., Bielas, J.H., Rabinovitch, P.S., Prolla, T.A., Loeb, L.A., 2008. DNA deletions and clonal mutations drive premature aging in mitochondrial mutator mice. *Nat. Genet.* 40, 392–394.
- Wallace, D.C., 2010. Mitochondrial DNA mutations in disease and aging. *Environ. Mol. Mutagen.* 51, 440–450.
- Wang, Z., Chesler, N.C., 2012. Role of collagen content and cross-linking in large pulmonary arterial stiffening after chronic hypoxia. *Biomech. Model. Mechanobiol.* 11, 279–289.
- Wang, Z., Kristianto, J., Yen Ooi, C., Johnson, M.G., Litscher, S.J., Pugh, T.D., Sandhu, G., Chesler, N.C., Blank, R.D., 2013a. Blood pressure, artery size, and artery compliance parallel bone size and strength in mice with differing *ecce1* expression. *J. Biomech. Eng.* 135, 61003–61009.
- Wang, Z., Lakes, R.S., Golob, M., Eickhoff, J.C., Chesler, N.C., 2013b. Changes in large pulmonary arterial viscoelasticity in chronic pulmonary hypertension. *PLoS One* 8, e78569.
- Weisbrod, R.M., Shiang, T., Al Sayah, L., Fry, J.L., Bajpai, S., Reinhart-King, C.A., Lob, H.E., Santhanam, L., Mitchell, G., Cohen, R.A., Seta, F., 2013. Arterial stiffening precedes systolic hypertension in diet-induced obesity. *Hypertension* 62, 1105–1110.
- Wolinsky, H., 1971. Effects of hypertension and its reversal on the thoracic aorta of male and female rats. Morphological and chemical studies. *Circ. Res.* 28, 622–637.
- Xue, B., Pamidimukkala, J., Hay, M., 2005. Sex differences in the development of angiotensin II-induced hypertension in conscious mice. *Am. J. Physiol.: Heart Circ. Physiol.* 288, H2177–H2184.
- Zhang, D., Mott, J.L., Chang, S.W., Denniger, G., Feng, Z., Zassenhaus, H.P., 2000. Construction of transgenic mice with tissue-specific acceleration of mitochondrial DNA mutagenesis. *Genomics* 69, 151–161.
- Zhang, D., Mott, J.L., Farrar, P., Ryerse, J.S., Chang, S.W., Stevens, M., Denniger, G., Zassenhaus, H.P., 2003. Mitochondrial DNA mutations activate the mitochondrial apoptotic pathway and cause dilated cardiomyopathy. *Cardiovasc. Res.* 57, 147–157.